Inorganic Chemistry

ARTICLE

pubs.acs.org/IC

Solution Synthesis of Nanoparticular Binary Transition Metal Antimonides

Gregor Kieslich,[†] Christina S. Birkel,[†] Andrew Stewart,[‡] Ute Kolb,[‡] and Wolfgang Tremel*[,†]

[†]Institut für Anorganische Chemie und Analytische Chemie der Johannes Gutenberg-Universität, Duesbergweg 10-14, D-55099 Mainz, Germany

[‡]Institut für Physikalische Chemie der Johannes Gutenberg-Universität, Welderweg 11, D-55099 Mainz, Germany

Supporting Information

ABSTRACT: The preparation of nanoengineered materials with controlled nanostructures, for example, with an anisotropic phase segregated structure or a regular periodicity rather than with a broad range of interparticle distances, has remained a synthetic challenge for intermetallics. Artificially structured materials, including multilayers, amorphous alloys, quasicrystals, metastable crystalline alloys, or granular metals, are mostly prepared using physical gas phase procedures. We report a novel, powerful solution-mediated approach for the formation of nanoparticular binary antimonides based on presynthesized antimony nanoparticles. The transition metal antimonides M−Sb (M = Co, Ni, Cu_2, Zn) were obtained with sizes ranging from 20 and 60 nm. Through careful control of the reaction conditions, single-phase nanoparticular antimonides were synthesized. The nanophases were investigated by powder X-ray diffraction and (high resolution) electron microscopy. The approach is based on activated metal nanoparticles as precursors for the synthesis of the intermetallic compounds. X-ray powder diffraction studies of reaction intermediates allowed monitoring of the reaction kinetics. The small particle size of the reactants ensures short diffusion paths, low activation barriers, and low reaction temperatures, thereby eliminating solid−solid diffusion as the rate-limiting step in conventional bulk-scale solid-state synthesis.

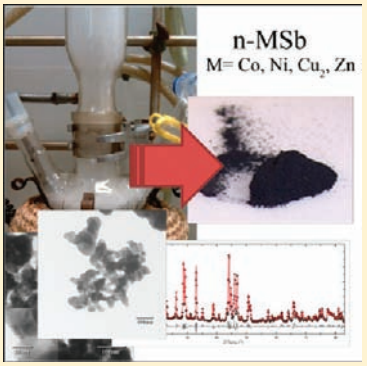

INTRODUCTION

During the past few decades transition metal antimonides have attracted much industrial and academic interest. They are among the parent compounds in crystal chemistry, and their great variety of electrical and magnetic properties originating from the variable compositions makes them interesting materials in metallurgy and solid state science.

Their properties include, for example, superconducting behavior[1−4] and the potential for use as lithium ion battery anode materials.[5−7] In addition, many binary and ternary antimonides have recently been identified as promising thermoelectric materials.[8−13] Material scientists are currently working on the reinvestigation of known compounds as well as on the de novo design of new compounds with the desired physical properties, that is, a large Seebeck coefficient and electrical conductivity and small thermal conductivity.[14]

Furthermore, low-dimensional materials and nanomaterials are known to exhibit properties that are fundamentally different from those of the corresponding bulk compounds, and many research groups focus on the synthesis of tailor-made nanoparticles with distinct chemical and physical properties. In the field of thermoelectrics, for example, much interest has been devoted to down-scaling well-known high performance bulk phases to further improve the figure of merit.[15−17]

Binary transition metal antimonides adopt very different crystal structures, thereby offering a wide variety of possible thermoelectric systems.[18,19] Compounds, such as $CoSb_3$, $FeSb_2$, and Zn_4Sb_3, have long been characterized as promising materials in thermoelectric devices.[20−22] NiSb and ZnSb show promising thermoelectric properties, as well.[14,23,24] To further investigate possible candidates within the antimonide family, phase pure nanoparticular samples must be prepared and characterized. The synthesis of intermetallic compounds usually requires high reaction temperatures and long reaction times for the thermodynamically stable phase to be formed. However, when this reaction temperature exceeds the corresponding nucleation energy of an intermediate phase, this phase is not accessible by classical solid state reactions. Besides, nanoparticles are sensitive to heat because of crystal growth during longer heating periods. The number of low temperature synthesis methods for nanocrystalline intermetallic compounds of the late transition metals has increased dramatically over the past few years. In situ reduction in high boiling solvents, (modified) polyol processes,[25,26] and solvothermal reaction processes allow the synthesis of metastable intermetallic phases.[27,28] However, the preparation of nanocrystalline antimonides has not been focused on extensively.[5,29−31] Therefore, we have optimized a low-temperature solution chemistry route allowing the formation of intermediate and metastable

Received: January 12, 2011
Published: July 07, 2011

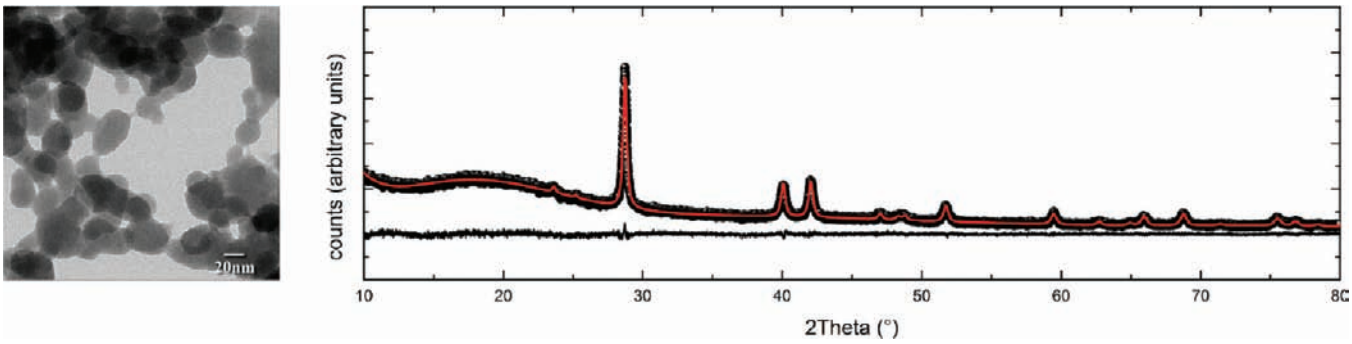

Figure 1. Antimony precursor particles: (a) TEM image showing agglomerated particles with sizes ranging 20−50 nm; (b) powder X-ray diffraction data (black dots), Rietveld refinement (red line), and corresponding difference curve of antimony precursor nanoparticles.

Table 1. Reaction Conditions for the Synthesis of the Late Transition Metal Antimonides

compd	metal precursor	solvent	reaction temperature (°C)	heating rate (°C/min)
CoSb	$Co_2(CO)_8$	tetraethyleneglycol	280	5
NiSb	Ni NP	tetraethyleneglycol	180	5
Cu_2Sb	Cu NP	trioctylamine	160	5
ZnSb	Zn NP	trioctylamine	300	15

antimony intermetallic phases. A new, metastable, and hitherto unknown Zn−Sb compound has been synthesized and identified.[28]

In the present study, we have extended this synthetic approach to the binary antimonides CoSb, NiSb, Cu_2Sb, and ZnSb to demonstrate its potential to access various compounds within the metal antimonide family. In contrast to the well-established polyol process, we start from metal particles and/or carbonyl precursors; that is, no additional salts (from reducing agents) or organic compounds are present in the syntheses (besides possible organic impurities in the used solvents). Therefore, this method can yield products without further impurities. In addition, this synthesis route allows the production of macroscopic masses of single-phase nanopowders and therefore allows further investigations of the thermoelectric properties.

The antimonides M−Sb (M = Co, Ni) adopt the NiAs-type crystal structure with the hexagonal space group $P6_3/mmc$. The structure can be described as a *hcp* arrangement of antimony atoms with the metal atoms filling the octahedral voids.[32] Cu_2Sb crystallizes in the anti-PbFCl structure with the tetragonal space group $P4/nmm$.[32] ZnSb crystallizes in the orthorhombic ZnSb structure (space group *Pbca*), as reported in 1948.[33] Both Zn and Sb adopt a 5-fold coordination by one like and four unlike neighboring atoms.[34]

RESULTS AND DISCUSSION

Synthesis. The synthetic approach we present here is based on the reaction of activated metal nanoparticles in a high-boiling solvent and has been described for the successful synthesis of metastable $Zn_{1+\delta}Sb$ before. Antimony nanoparticles are either reacted with other metal nanoparticles or reacted with a molecular metal precursor and are produced by reduction of $SbCl_3$ in lithium triethylboronhydride $Li[Et_3BH]$ at room temperature in tetrahydrofuran (THF). Activated Sb nanoparticles are highly reactive in ambient air, leading primarily to the formation of Sb_2O_3. ^1H NMR data of Sb nanoparticles kept in an inert gas atmosphere show an intense signal according to surface bond stibane ($\delta \approx 1.05$ ppm), which broadened when the particles were in contact with air, cf. Figures SI-1 and SI-2 in the Supporting Information. In the case of antimony, it is very difficult to obtain well separated, monodisperse nanoparticles. Nevertheless, this synthetic technique was studied to obtain intermetallic binary antimonides for a proof of principal study with a focus on the thermal conductivity. Note that we report exclusively on the synthesis and characterization of the nanoparticles, which will be used for subsequent studies of lattice dynamics. Therefore, the interface density is important. To perform detailed physical property measurements, the powders need to be compacted into a pellet. There are reports of well-dispersed antimony nanoparticles and wires, prepared in high dilution polyol processes,[35] which might not be suitable for further reactions with other transition metal nanoparticles or carbonyls. Schlecht et al. reported the synthesis of ZnSb and Zn_4Sb_3 nanoparticles from activated Sb nanoparticles in a fused silica ampule.[36] We are using these activated particles in solution based syntheses, which allows us to study the influence of additional reaction parameters on the forming antimonide nanoparticles. Therefore, the activated nature of the nanoparticles without any capping agents or polymers on their surface is of great importance. A TEM image and a powder XRD profile of the activated Sb nanoparticles are provided in Figure 1. The refined lattice parameters (a = 4.29 nm, c = 11.29 nm, r_wp = 4.9, r_Bragg = 0.57) fit well to the reported bulk parameters.[37] Furthermore, the calculated average crystallite size of approximately 37 nm matches the crystallite sizes obtained from TEM images.

Ni, Zn, and Cu nanoparticles were prepared from the corresponding chlorides. The resulting elemental nanoparticles were characterized by electron microscopy to verify the nanosize of the corresponding elemental particles. For the synthesis of NiSb, ZnSb, and Cu_2Sb nanoparticles, the corresponding metal particles were dispersed in a high-boiling solvent and added to the solution of antimony nanoparticles, and the mixture was heated to temperatures between 150° and 300 °C. Antimony nanoparticles and $Co_2(CO)_8$ were reacted with each other to form CoSb. Starting from $Co_2(CO)_8$ as cobalt precursor eliminates the reduction step and enables a high purity of the resulting CoSb nanoparticles. Similar precursors for the other metals could not be used in the reported synthesis. Presynthesized Co nanoparticles did not lead to the formation of a phase pure compound.

With the help of the powder X-ray diffraction data of the reaction intermediates, the reaction conditions for the formation

dx.doi.org/10.1021/ic200074z |*Inorg. Chem.* 2011, 50, 6938–6943

of the different antimonides were optimized in terms of (shortest) reaction time, phase purity, and crystallinity. The results are summarized in Table 1. In all cases, Sb nanoparticles that react with different metal precursors at different reaction temperatures were used. It should be noted that the reported final reaction temperatures are the lowest possible ones allowing the formation of phase pure nanoparticles within an acceptable time frame (<12 h).

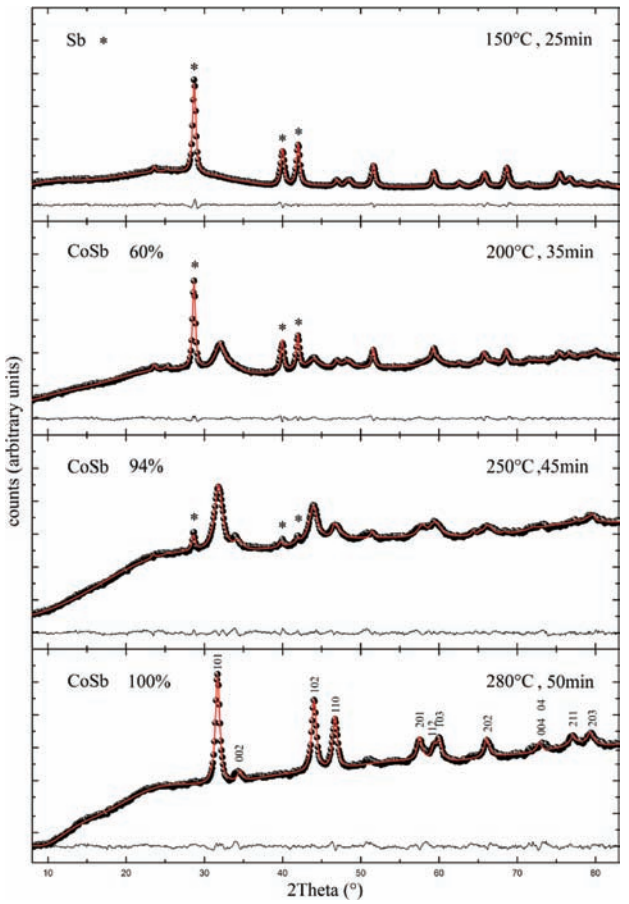

Figure 2. Formation of CoSb. Time-dependent and temperature-dependent (ex situ) X-ray diffraction: experimental data (black dots), Rietveld fits (red line), and corresponding difference plots (black line) at different reaction temperatures and times.

By starting from small metal particles, solid state diffusion is no longer the rate-limiting step of the reaction and different phases are accessible. In contrast to conventional solid state reactions that allow the formation of the thermodynamically stable product, nanostructured metastable[28] and intermediate compounds can be made by this approach. However, this synthesis approach is highly sensitive to a variety of parameters, such as heating rate, final temperature, reaction time, solvent, and precursor material. On the other hand, this variety of reaction conditions also allows an optimization of the reaction process to obtain the target phase. In the case of NiSb, Cu_2Sb, and ZnSb, metal nanoparticles could be used as precursor materials, whereas CoSb could only be obtained with $Co_2(CO)_8$ as starting compound. Additionally, for CoSb, Cu_2Sb, and ZnSb, only the solvent shown in Table 1 led to the formation of phase pure material, whereas for NiSb the solvent seems to have a minor influence. The NiSb phase was also obtained if other solvents (trioctylamine, triethylenegylcol) were used. One reason for the higher flexibility of the synthesis conditions for NiSb could be its rather broad phase width compared to those of the other compounds described here. In a typical synthesis of NiSb, tetraethyleneglycol was used as a solvent.

Powder X-ray Diffraction. X-ray powder diffraction profiles of all compounds recorded from the reaction intermediates and the final products (Figure 2 and Figures SI-3 and SI-4 in the Supporting Information) revealed that all target phases form during the heating step.

For the synthesis of CoSb, Sb was consumed upon further heating. The reaction yields pure CoSb at 280 °C. For NiSb, Cu_2Sb, and ZnSb the target phases and precursor compounds were crystalline at the final temperature and subsequently reacted to form the final product.

As mentioned above, the resulting nanoparticle phases and the product distribution strongly depend upon the reaction conditions,

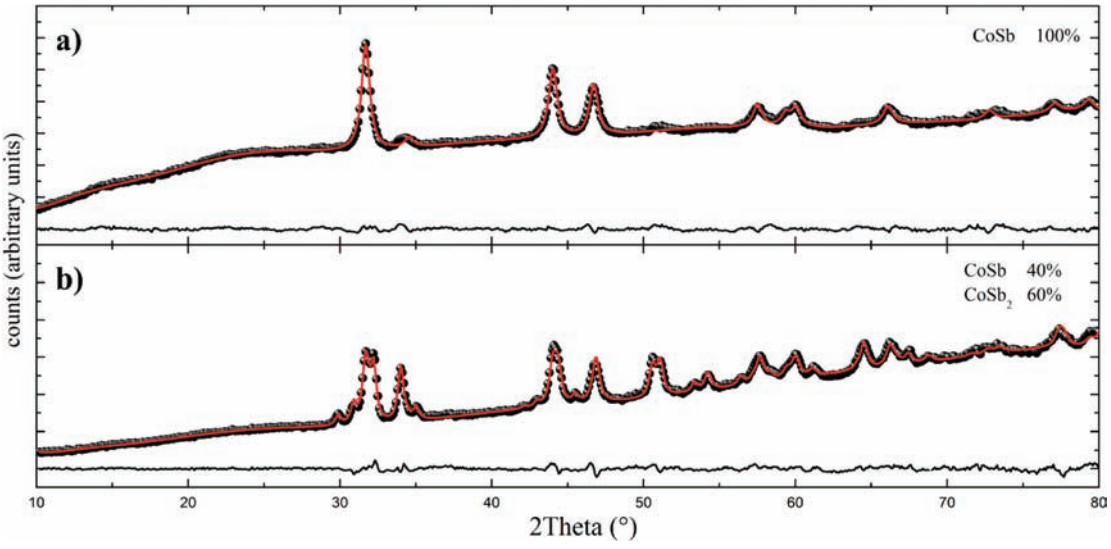

Figure 3. Influence of the heating rate on the composition of the $CoSb/CoSb_2$ system. Experimental data (black dots), Rietveld fits (red line), and corresponding difference plots (black line). (a) Optimized heating rate, 5 K/min, yields phase pure CoSb. (b) Heating rate 15 K/min yields a mixture of CoSb and $CoSb_2$. Excess Co was removed with 1 M HCl.

dx.doi.org/10.1021/ic200074z |*Inorg. Chem.* 2011, 50, 6938–6943

Table 2. Refined Lattice Parameters for the Obtained Compounds and Literature Values (The corresponding references are given in the text.)

compd	reported lattice parameters (bulk)	refined lattice parameters (nano) ± error	calcd avg crystallite size ± error	r_wp (r_Bragg)
CoSb	$a = 3.890$	$a = 3.899 \pm 0.001$	16.14 ± 0.38	2.278
	$c = 5.186$	$c = 5.207 \pm 0.002$		(1.31)
NiSb	$a = 3.934$	$a = 3.934 \pm 0.001$	12.75 ± 0.14	5.481
	$c = 5.138$	$c = 5.145 \pm 0.001$		(1.53)
Cu_2Sb	$a = 4.001$	$a = 4.008 \pm 0.0003$	33.84 ± 0.60	2.805
	$c = 6.104$	$c = 6.112 \pm 0.001$		(0.89)
ZnSb	$a = 6.202$	$a = 6.214 \pm 0.0003$	82.13 ± 1.82	5.17
	$b = 7.742$	$b = 7.756 \pm 0.0004$		(2.07)
	$c = 8.100$	$c = 8.098 \pm 0.0004$		

and they are sensitive toward variation of these variables. The most important reaction parameters are (i) overall reaction time, (ii) final temperature, and (iii) heating rate. The overall reaction time seems to control the progress of the reaction between the antimony nanoparticles and the metal precursors. Thus, short reaction times result in impurities of unreacted antimony. The final temperature and heating rate control the phase formation and the phase purity as shown in Figure 3 for the $CoSb/CoSb_2$ system. In a similar way, variations of the synthesis parameters lead to the formation of $NiSb_2$ impurities during the synthesis of NiSb. Although the MSb_2 (M = Co, Ni) phases often appeared as impurity phases, no appropriate reaction conditions for the formation of phase pure compounds $CoSb_2$ and $NiSb_2$ could be found so far. The synthesis of Cu_2Sb is prone to antimony impurities, but long reaction times (>180 min) could solve this general problem and allow the synthesis of single-phase Cu_2Sb. For ZnSb, the major impurity is the $Zn_{1+\delta}Sb$ phase and the corresponding, optimized reaction conditions have been reported.[28] The formation of antimony impurities is observed in most cases, and the synthesis of ZnSb is, therefore, the most delicate procedure reported here.

All quantitative phase analyses plotted in Figure 2 and Figures SI-3, SI-4, and SI-5 in the Supporting Information were performed by full pattern profile analyses of the corresponding X-ray diffraction data using the published structural data for CoSb, NiSb,[38] Cu_2Sb,[39] ZnSb,[40] and Sb,[37] respectively, using TOPAS Academic V 4.1.[41] We considered the observed data with caution, and the results of the refinements are given in Table 2. In all refinements there were no hints of defects or nonstiochiometry of the end products. Therefore, the atom positions were not refined. In all cases the refined lattice parameters of the nanopowders fit to the reported parameters of the corresponding bulk phases (cf. Table 2).

Transmission Electron Microscopy. Transmission electron microscopy images of the different nanoparticular compounds shown in Figure 4 revealed the presence of highly agglomerated nanoparticles. Despite intensive sonication during TEM sample preparation, individual crystals were never observed, and even the smallest aggregates consisted of several crystals.

The sizes of the nanoparticles ranged from 20 nm to approximately 60 nm. Most nanoparticles revealed isotropic shapes, but anisotropic structures were found in the case of the Cu_2Sb (Figure 4c).

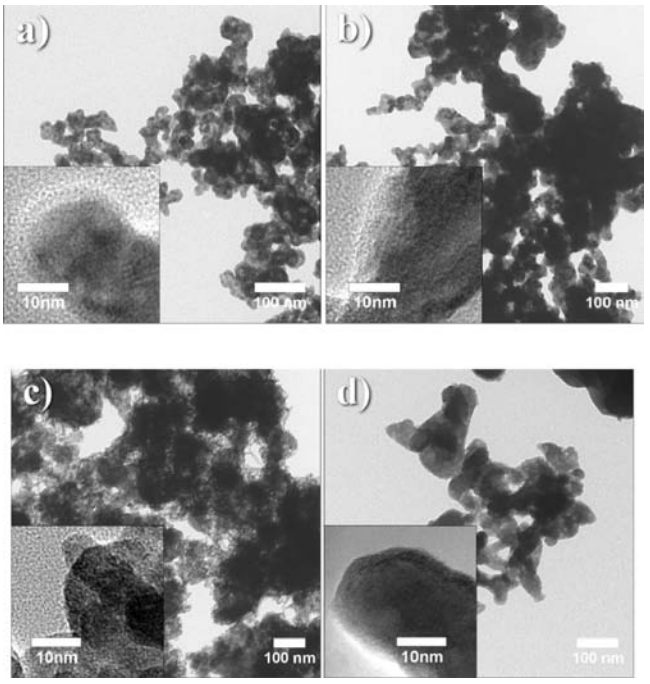

Figure 4. TEM micrographs of the nanostructured compounds: (a) CoSb, (b) NiSb, (c) Cu_2Sb, and (d) ZnSb.

In general, the particle sizes observed by TEM are overestimated with respect to the refined crystallite sizes. Taking into account that the refined crystallite sizes of X-ray diffraction data are average values and that the particle size is not strictly equal to the crystallite size, there is a satisfactory agreement between the results of the X-ray diffraction and electron microscopy studies.

CONCLUSION

In this contribution, we have extended the strategy that was demonstrated for the solution synthesis of nanoparticular $Zn_{1+\delta}Sb$ to a general solution-mediated synthesis of nanocrystalline binary antimonides.[28] Our approach, the result of ongoing investigations of reaction pathways in the synthesis of intermetallics, involves a low-temperature chemical conversion of preformed activated antimony via reaction of (i) organometallic precursors such as metal carbonyls or (ii) metal nanocrystals into intermetallics. This strategy, yielding morphologically controllable nanocrystalline intermetallics starting from commercially available reagents, appears very general. This work complements the previous work reported by other groups[30−32,36,42,43] for the synthesis of nanocrystalline intermetallics by providing an alternative access that is general and robust. The small particle size of the reactants ensures short diffusion paths, low activation barriers, and low reaction temperatures, thereby eliminating solid−solid diffusion as the rate-limiting step in conventional bulk-scale solid-state synthesis. The high flexibility of this synthetic route in terms of reaction parameters allows for easy control over accessible phases and structures. We think that this is a powerful strategy for the synthesis of diverse nanoparticular intermetallics with a large potential in different applications.

EXPERIMENTAL SECTION

Synthesis of the Metal Nanoparticles. $ZnCl_2$ (ABCR, 99.999%), $NiCl_2$ (Sigma-Aldrich, 99.99%), and CuCl (ABCR, 99.995%)

were first dried with thionylchloride, washed with toluene, dried in vacuum, and stored in a glovebox under N_2 atmosphere. Tetrahydrofuran was dried with $CaCl_2$ and Na/K and freshly distilled before use. Lithium triethylboronhydride Li[Et_3BH] (Aldrich, 1 M in THF, referred to as "superhydride") and $SbCl_3$ (ABCR, 99.99%) were used as obtained, and $SbCl_3$ was stored in a glovebox. Zn particles were synthesized by the reaction of $ZnCl_2$ with 2 equiv of the 1 M solution of superhydride in THF at ~65 °C. The particles were washed several times with THF, dried in a vacuum, and stored in a glovebox. Sb particles, Ni particles, and Cu particles were produced by reducing $SbCl_3$, $NiCl_2$, and CuCl with 3, 2, and 1 equiv of the 1 M superhydride solution at room temperature, respectively. The black particles were repeatedly redispersed in THF and decanted from the solution, dried in a vacuum, and kept in a glovebox.

Synthesis of Binary Antimonide Nanoparticles. Trioctylamine and tetraethyleneglycol (Aldrich, 98%) were degassed and stored under Ar before use.

CoSb. In a typical synthesis, nanoparticles of the nominal composition CoSb were prepared by heating of Sb-nanoparticles (1 mmol) and $Co_2(CO)_8$ (0.5 mmol) in tetraethyleneglycol (ultrasound bath for 10 min) with a heating rate of about 5 K/min. The reaction mixture was heated to ca. 280 °C. For intermediate products, 2 mL of the solution was extracted by syringe at approximately 150, 200, 250, and 280 °C. After the solution was cooled to room temperature, the resulting black product was collected by centrifugation (9000 rpm), washed with ethanol, and dried under a steady Ar flow.

NiSb. In a typical synthesis, nanoparticles of the nominal composition NiSb were prepared by heating of Sb-nanoparticles (1 mmol) and Ni-nanoparticles (1 mmol) in tetraethyleneglycol (ultrasound bath for 10 min) with a heating rate of about 5 K/min. The reaction mixture was heated to ca. 170 °C and held there 210 min. For intermediate products, 2 mL of the solution was extracted by syringe at approximately 70, 80, 140, and 170 °C. After the solution was cooled to room temperature, the resulting black product was collected by centrifugation (9000 rpm), washed with ethanol, and dried under a steady Ar flow.

Cu_2Sb. In a typical synthesis, nanoparticles of the nominal composition Cu_2Sb were prepared by heating of Sb-nanoparticles (1 mmol) and Cu-nanoparticles (2 mmol) in tricotylamine (ultrasound bath for 10 min) with a heating rate of about 5 K/min. The reaction mixture was heated to ca. 160 °C and held there for 180 min. For intermediate products, 2 mL of the solution was extracted by syringe at approximately 50 and 100 °C. After the solution was cooled to room temperature, the resulting black product was collected by centrifugation (9000 rpm) and washed with ethanol. Afterward, the black powder was washed two times with 1 M HCl in saturated NH_4Cl solution to remove possible Cu residues. The powder was then again washed with ethanol and dried under a steady Ar flow.

ZnSb. In a typical synthesis, Sb- and Zn-nanoparticles were heated to 300 °C at a rate of ca. 15 K/min in a polar, strongly coordinating solvent (trioctylamine) to prevent nanoparticle aggregation. The reaction mixture was held at ca. 300 °C for 60 min before it was allowed to cool down. Products were collected by centrifugation, washed with ethanol, and subsequently dried in vacuo. The syntheses had to be carried out using an excess (3:1) of zinc metal to ensure all Sb reacted to form the desired product. The additional Zn can be removed after the reaction by repeated treatment of the solid residue with dilute acetic acid. The product was then washed with ethanol and dried with streaming Ar to a dry powder.

X-ray Powder Diffraction. X-ray powder diffraction data were collected with a Bruker-AXS D8-Discover diffractometer in reflection geometry equipped with a HiStar detector using graphite monochromatized Cu Kα radiation. Samples were glued on top of glass and (111) silicon substrates, respectively, using VP/VA copolymer (vinylpyrrolidone/vinylacetate). Rietveld refinements were performed with TOPAS Academic v4.1[41] applying the fundamental parameter approach.

Transmission Electron Microscopy. For TEM investigations the sample was suspended in ethanol and dropped onto a carbon coated copper grid. The images were obtained using a Philips EM420 instrument with an acceleration voltage of 120 kV.

For HRTEM investigations the sample was also suspended in ethanol and sprayed onto a carbon coated copper grid using the sonifier described in ref 44. The TEM work was carried out with a Tecnai F30 S-TWIN transmission electron microscope equipped with a field emission gun working at 300 kV. High-resolution (HR-) TEM and electron diffraction patterns were acquired with a CCD camera (14-bit GATAN 794MSC).

■ ASSOCIATED CONTENT

Supporting Information. (1) ^{1}H NMR data of Sb, measured under Ar; (2) ^{1}H NMR data of Sb, measured under ambient air; time-dependent and temperature-dependent (ex situ) X-ray diffraction plots of (3) formation of NiSb and (4) formation of Cu_2Sb; (5) X-ray diffraction, Rietveld refinements, and corresponding difference plots of the final ZnSb product. This material is available free of charge via the Internet at http://pubs.acs.org.

■ AUTHOR INFORMATION

Corresponding Author

*Phone: +49 6131 392-5135. Fax: +49 6131 392-5605. E-mail: tremel@uni-mainz.de.

■ ACKNOWLEDGMENT

This research was supported by the DFG priority program SPP1386 Nanostructured Thermoelectrics. C.S.B. and G.K. are recipients of a fellowship from MATCOR, the Graduate School of Excellence of the State of Rhineland-Palatinate.

■ REFERENCES

(1) Matthias, B. T. *Phys. Rev.* **1953**, *92*, 874–876.
(2) Matthias, B. T.; Geballe, T. H.; Compton, V. B. *Rev. Mod. Phys.* **1963**, *35*, 1–&.
(3) Matthias, B. T.; Compton, V. B.; Corenzwit, E. *J. Phys. Chem. Solids* **1961**, *19*, 130–133.
(4) Bukowski, Z.; Badurski, D.; Stepien-Damm, J.; Troc, R. *Solid State Commun.* **2002**, *123*, 283–286.
(5) Xie, J.; Zhao, X. B.; Yu, H. M.; Qi, H.; Cao, G. S.; Tu, J. P. *J. Alloys Compd.* **2007**, *441*, 231–235.
(6) Wang, M.; Zhao, H.; He, J.; Wang, R.; Chen, J.; Chen, N. *J. Alloys Compd.* **2009**, *484*, 864–869.
(7) Villevieille, C.; Ionica-Bousquet, C. M.; de Benedetti, A. Morato, F.; Pierson, J. F.; Simon, P.; Monconduit, L. *Solid State Ionics* [Online early access]. DOI: 10.1016/j.ssi.2010.03.019. Published Online: June 7, 2010.
(8) McGuire, M. A.; Reynolds, T. K.; DiSalvo, F. J. *J. Alloys Compd.* **2006**, *425*, 81–87.
(9) Meng, J. F.; Polvani, D. A.; Jones, C. D.; DiSalvo, F. J.; Fei, Y.; Badding, J. V. *Chem. Mater.* **2000**, *12*, 197–201.
(10) Jones, C. D.; Regan, K. A.; DiSalvo, F. J. *Phys. Rev. B* **1998**, *58*, 16057–16063.
(11) Brown, S. R.; Kauzlarich, S. M.; Gascoin, F.; Snyder, G. J. *Chem. Mater.* **2006**, *18*, 1873–1877.
(12) Cox, C. A.; Brown, S. R.; Snyder, G. J.; Kauzlarich, S. M. *J. Electron. Mater.* **2010**, *39*, 1373–1375.
(13) Rauscher, J. F.; Cox, C. A.; Yi, T.; Beavers, C. M.; Klavins, P.; Toberer, E. S.; Snyder, G. J.; Kauzlarich, S. M. *Dalton Trans.* **2010**, *39*, 1055–1062.

(14) Snyder, G. J.; Toberer, E. S. *Nat. Mater.* **2008**, *7*, 105–114.
(15) Hicks, L. D.; Dresselhaus, M. S. *Phys. Rev. B* **1993**, *47*, 12727–12731.
(16) Hicks, L. D.; Dresselhaus, M. S. *Phys. Rev. B* **1993**, *47*, 16631–16634.
(17) Hicks, L. D.; Harman, T. C.; Dresselhaus, M. S. *Appl. Phys. Lett.* **1993**, *63*, 3230–3232.
(18) Tremel, W.; Hoffmann, R.; Silvestre, J. *J. Am. Chem. Soc.* **1986**, *108*, 5174–5187.
(19) Hulliger, F. In *Structure and Bonding*; Springer: New York, 1968; Vol. 4.
(20) Sootsman, J.; Chung, D.; Kanatzidis, M. *Angew. Chem., Int. Ed.* **2009**, *48*, 8616–8639.
(21) Bentien, A.; Johnsen, S.; Madsen, G. K. H.; Iversen, B. B.; Steglich, F. *Europhys. Lett.* **2007**, *80*, 17008–17012.
(22) Kleinke, H. *Chem. Mater.* **2010**, *22*, 604–611.
(23) Li, C.; Hu, J.; Wang, X. *Mater. Chem. Phys.* **2008**, *110* (1), 106–109.
(24) Shaver, P. J.; Blair, J. *Phys. Rev.* **1966**, *141*, 649.
(25) Leonard, B. M.; Bhuvanesh, N. S. P.; Schaak, R. E. *J. Am. Chem. Soc.* **2005**, *127*, 7326–7327.
(26) Schaak, R. E. *Abstr. Pap., Am. Chem. Soc.* **2005**, *229*, U965–U965.
(27) Cushing, B. L.; Kolesnichenko, V. L.; O'Connor, C. J. *Chem. Rev.* **2004**, *104*, 3893–3946.
(28) Birkel, C. S.; Mugnaioli, E.; Gorelik, T.; Kolb, U.; Panthoefer, M.; Tremel, W. *J. Am. Chem. Soc.* **2010**, *132*, 9881–9889.
(29) Kobayashi, H.; Kageshima, M.; Kimura, N.; Aoki, H.; Oohigashi, M.; Motizuki, K.; Kamimura, T. *J. Magn. Magn. Mater.* **2004**, *272−276*, 247–248.
(30) Cable, R. E.; Schaak, R. E. *Chem. Mater.* **2005**, *17*, 6835–6841.
(31) Kumari, L.; Li, W.; Huang, J. Y.; Provencio, P. P. *J. Phys. Chem. C* **2010**, *114*, 9573–9579.
(32) Kift, R. L.; Prior, T. J. *J. Alloys Compd.* **2010**, *505*, 428–433.
(33) Almin, K. E. *Acta Chem. Scand.* **1948**, *2*, 400–407.
(34) Mikhaylushkin, A. S.; Nylen, J.; Haussermann, U. *Chem.—Eur. J.* **2005**, *11*, 4912–4920.
(35) Wang, Y. W.; Hong, B. H.; Lee, J. Y.; Kim, J.-S.; Kim, G. H.; Kim, K. S. *J. Phys. Chem. B* **2004**, *108*, 16723–16726.
(36) Schlecht, S.; Erk, C.; Yosef, M. *Inorg. Chem.* **2006**, *45*, 1693–1697.
(37) Degtyareva, V. F. *J. Synchrotron Radiat.* **2005**, 584–589.
(38) Kjekshus, A.; Walseth, K. P. *Acta Chem. Scand.* **1969**, *23*, 2621–2630.
(39) Pearson, W. B. *Can. J. Phys.* **1964**, *42*, 519–525.
(40) Carter, F. L.; Mazelsky, R. *J. Phys. Chem. Solids* **1964**, *25*, 571–&.
(41) Coelho, A. *TOPAS Academic*, V1.0; Coelho Software: Brisbane, Australia, 2004.
(42) Chou, N. H.; Schaak, R. E. *J. Am. Chem. Soc.* **2007**, *129*, 7339–7345.
(43) Alden, L. R.; Han, D. K.; Matsumoto, F.; Abruna, H. D.; DiSalvo, F. J. *Chem. Mater.* **2006**, *18*, 5591–5596.
(44) Mugnaioli, E.; Gorelik, T.; Kolb, U. *Ultramicroscopy* **2009**, *109*, 758–765.